Experimental Thermal and Fluid Science 108 (2019) 104–114

Contents lists available at ScienceDirect

Experimental Thermal and Fluid Science

journal homepage: www.elsevier.com/locate/etfs

Collapse dynamics of bubble pairs in gelatinous fluids☆

Thomas Hopfes*, Zhaoguang Wang, Marcus Giglmaier, Nikolaus A. Adams

Chair of Aerodynamics and Fluid Mechanics, Technical University of Munich, Boltzmannstr. 15, D-85748 Garching bei München, Germany

ARTICLE INFO

Keywords:
Experimental bubble dynamics
Gelatin
Shock tube
Bubble pairs

ABSTRACT

Bubble dynamics is relevant in a variety of research fields that range from material science to medical applications. It is studied extensively, and researchers apply very established and reliable experimental methods. Although these methods provide many advantages and are constantly modified and adapted, there are also some limitations on which aspects can be analyzed. Thus, we present in this study a novel experimental setup that uses a shock tube and applies a gelatinous mixture as a water-like carrier medium. Millimeter-sized air bubbles, placed in the gelatin and exposed to an instantaneous pressure increase, are analyzed under two different aspects. First, we show that single bubbles in the gelatin behave very similarly to bubbles in water during the collapse and that different gelatin concentrations do not significantly affect the behavior. In a second part, we study interacting bubble pairs and differentiate four main types of interaction that can also be characterized by non-dimensional parameters. A well-known type, jetting towards each other, is reproduced and a type termed 'reversing collapse' shows similarities to previous work as well as new aspects. The interaction of bubbles of large size ratios is either dominated by the large bubble if bubbles are far apart or leads to a pronounced liquid jet if the bubbles are close to each other. The presented results demonstrate that the applied experimental setup can provide insight into bubble interaction and jet formation. This could help, for example, to establish controlled and directed jetting of microbubbles in targeted drug delivery, which would play a major role in anticancer research.

1. Introduction

Research on bubble dynamics has a long history in fluid mechanics. Initially, cavitation and related phenomena were noticed due to their destructive potential, for example in the surface erosion on ship propellers [3]. However, there are not only adverse, but also beneficial aspects. Medical procedures, such as lithotripsy and targeted drug delivery, try not only to understand and avoid, but rather to exploit bubble dynamics. Lithotripsy, for example, is an established medical procedure for non-invasive destruction of gallstones in the human body by focusing extracorporeally generated shock waves on the target [4]. Cavitation bubbles are formed in the liquid surrounding the gallstone by a focused tensile wave that follows the preceding shock wave. These bubbles then interact with following shock waves and an aspherical collapse can lead to strong erosive effects through liquid jets and shock wave emission. Thus, transient cavitation is a dominant mechanism that strongly determines the overall effectiveness of the treatment [5]. One major idea behind targeted drug delivery is to use coated microbubbles as drug carriers in the human body. Ligands on the bubble surface target specific cells before ultrasound pressure pulses, generated outside the body, break the bubbles apart and release the carried drug at the targeted location [6].

To improve the mentioned applications, bubble dynamics has been studied extensively. Fong et al. [7] speak of three widely used experimental methods to generate oscillating cavitation bubbles under reasonably controlled conditions: laser-focus, spark discharge and acoustic waves. They mention, however, that acoustic waves do not allow a high-level of accuracy for bubble positioning. In contrast, laser-generated cavitation is a very prominent method that is favored for its reproducibility and the ability to create nearly perfect spheres [8]. Cavities are created by focusing strong light pulses into a liquid, which creates a plasma at the focus point. The related phenomenon is called dielectric breakdown or, in the context of bubble generation, also optic cavitation [9]. Generating cavities with a laser has several major advantages. Cavities can be produced at any given time and at any accessible position in a liquid. It is therefore possible to produce cavities right before the impact of a shock wave [10], to change the distance of the bubble from a solid wall continuously [11] or to produce the bubble

☆ This work is based on two contributions that were presented at the 5th International Conference on Experimental Fluid Mechanics, Munich, Germany, July 2–4, 2018 [1,2].

* Corresponding author.
E-mail address: thomas.hopfes@tum.de (T. Hopfes).

https://doi.org/10.1016/j.expthermflusci.2019.05.023
Received 27 January 2019; Received in revised form 10 May 2019; Accepted 30 May 2019
Available online 31 May 2019

next to a spherical particle [12]. This technique can produce bubbles that are perfectly spherical, so that Obreschkow et al. [13] can even study the small effect of gravity-induced pressure gradients on bubble collapse during parabolic flights. Spark generation is an alternative method that has been widely used for bubble dynamic experiments by many researchers [14–17]. It uses wires to discharge electric energy, which again leads to the formation of a plasma point that then expands to form the cavitation bubble. In general, both methods are well established and provide similar advantages and restrictions. The processes work repeatedly, reliably and offer a high level of precision in respect to the bubble shape and position. However, the mentioned methods can only study vapor bubbles. Research on pure, non-condensable gas bubbles is rarer and often has other drawbacks. The applied bubbles are, for example, rising [18], attached to a solid surface [19–21] or have to be kept in position by other means (e.g. a plastic foil [22]). In addition, often very strong pressure pulses are used to collapse the bubbles in such setups. The pulses are created by micro-explosives [18,19,21], optical breakdown [20] or a lithotripter [22,23], which results in very short term pressure peaks, rather than a constant surrounding pressure.

A constant surrounding pressure and well-defined boundary conditions are, however, desirable. To achieve that, a novel experimental method is used for the present study. The approach relies on two aspects. First, a shock tube generates a planar shock front which provides an instantaneous pressure jump to a constant high pressure. Second, a gelatinous mixture is used as a water-like carrier medium to contain pure gas bubbles rather than vapor bubbles. This distinguishes the setup from experiments with gas bubbles under strong shock-loading and from research that uses vapor bubbles. The combination expands the methodology in bubble dynamics research, although both aspects – using a shock tube and placing bubbles in gelatin – have been used individually in previous studies (e.g. [24,25] and [26,27] respectively).

Some advantages can be achieved with the present setup. The initial configuration shows the bubble and surrounding gelatin completely at rest at atmospheric pressure. In addition, the gelatin is enclosed by rigid boundaries on all sides except at the interface to the air within the driven section of the shock tube. This creates a well-defined surrounding and conditions that are favorable when the experiments serve as a reference for numerical simulations. Another positive aspect is that multiple bubbles of different sizes and at various distances can be produced without additional effort. This allows a much better representation of application scenarios, where bubbles often are present in clusters and interact with each other.

The paper is structured so that Section 2 presents the general experimental setup. On a side note, Section 2.2 shows aspects of the different applied test sections and highlights the impact of fluid-structure interaction in experimental work on bubble dynamics. In Section 3, we discuss advantages and restrictions of the setup and analyze to what extent an increasing gelatin concentration affects bubble oscillation by comparing the results to the case of bubbles in water. First results of experiments on interacting bubble pairs are presented in Section 4, while Section 5 summarizes and concludes the present work.

2. Methods

2.1. Experiment

Fig. 2-1 shows a sketch of the experimental setup used in the present study. Main parts are the shock tube, the test section filled with the gelatin and the measurement equipment, such as pressure transducers and the optical system. The shock tube, with an overall length of 22.5 m and an inner diameter of 290 mm, consists of three parts: the driver, the driven and the test section. A diaphragm separates the high-pressure driver section (used in this study at pressures of up to 8 bar) from the driven section at atmospheric pressure (p_1). Upon diaphragm rupture, a shock wave is created which propagates towards the test section at shock Mach number M_S. It induces an instantaneous pressure and temperature rise as well as a flow velocity in the driven gas. The pressure behind the shock, p_2 can be calculated after [28] as

$$p_2 = p_1\left(1 + \frac{2\kappa}{\kappa+1}(M_s^2 - 1)\right) \tag{1}$$

with the heat capacity ratio of air, κ, taken at a value of $\kappa = 1.4$.

Fig. 2-2(a) shows the shock wave propagating into the test section of a cross section of 190 × 190 mm^2 that is partially filled with gelatin. A sketch shows the corresponding wave motion. When the shock wave arrives at the air-gelatin interface, it reflects almost ideally due to the high difference in acoustic impedance of the two materials and travels upstream at a shock Mach number M_R that can be calculated solely from M_S. The reflected shock causes the gas flow to halt and increases the pressure to $p_{2'}$ which can be calculated with Eq. (1) by substituting M_S with M_R and p_1 with p_2. Since the pressure must be equal at the interface, a compression wave propagates into the gelatin and increases the pressure to the value behind the reflected shock ($p_{2'}$). The compression wave reflects at the solid end wall of the test section, which further increases the pressure ($p_{2''}$). Assuming ideal wave motion and acoustic theory, the pressure increase over the reflected compression wave is equal to the increase over the initial compression wave, calculated as $\Delta p_{12'} = p_{2'} - p_1$, to lead to an ideal pressure increase at the back wall of $\Delta p_{\text{ideal}} = 2\Delta p_{12'}$. The pressure stays constant in the liquid and the bubbles, shown exemplarily in Fig. 2-2(b–c), collapse and oscillate. The constant conditions last until the reflected compression wave reaches the air-gelatin interface and reflects as an expansion wave that induces a pressure reduction. Consequently, the test time is limited to about 0.4 ms for a gelatin-filled test section of 300 mm length and a speed of sound in gelatin of $a_{\text{gel}} = 1500$ m/s. However, Section 2.2 will show that this ideal wave motion does not predict the measured pressure accurately. The pressure is affected by the type and rigidity of the used test section.

To create the gelatin, we dissolved Gelrite™ Gellan Gum within demineralized water and added magnesium sulfate ($MgSO_4$) after heating. The mixture was poured into the test section, cooled off and formed a clear, agar-like gelatin. In contrast to the ideal setup depicted in Fig. 2-2, a thin plastic foil was placed between gelatin and air since it significantly facilitates the handling of the gelatin without noticeable influencing the experiment. Bubbles were produced by first inserting the needle of a syringe through a small closable hole in the back wall and extracting a small amount of gelatin. The needle was removed and carefully inserted again to then release a defined amount of air. We found that bubbles of up to 1.5 mm radius could be produced in a very spherical shape, whereas bigger radii tended to enhance non-spherical deviations. After production, the bubbles rested under well-defined initial conditions such as constant pressure (p_1), constant temperature, and zero initial velocity until the experiment started. Bubbles were positioned near the centerline of the test section and thus were far from the side walls to avoid any interaction. To take advantage of the ideal pressure rise Δp_{ideal}, bubbles were positioned towards the end of the test section. However, the distance of the bubbles to the back wall was kept at around 10 times the bubble diameter to minimize wall effects [29].

For visualization, we applied a Z-type schlieren system without cutting light at the second focal point to create ‘focused shadowgraph’ images [30]. Powered by a 150 W constant Xenon light source, the optical system projected the visualized section along the line-of-sight on the camera focal plane. This gave a two-dimensional representation of the three-dimensional bubble. The collapse was recorded by a Shimadzu HyperVision HPV-X ultra-high-speed camera that produces videos of 128 consecutive frames with a resolution of 400 × 250 pixels at up to 5 million frames per second. Simultaneously, PCB Piezotronics ICP® fast-response pressure sensors, connected to an LTT transient recorder, monitored and recorded the pressure during the experiment at six locations at a frequency of 1 MHz per channel. Two sensors along the tube were always connected to allow accurate measurement of the

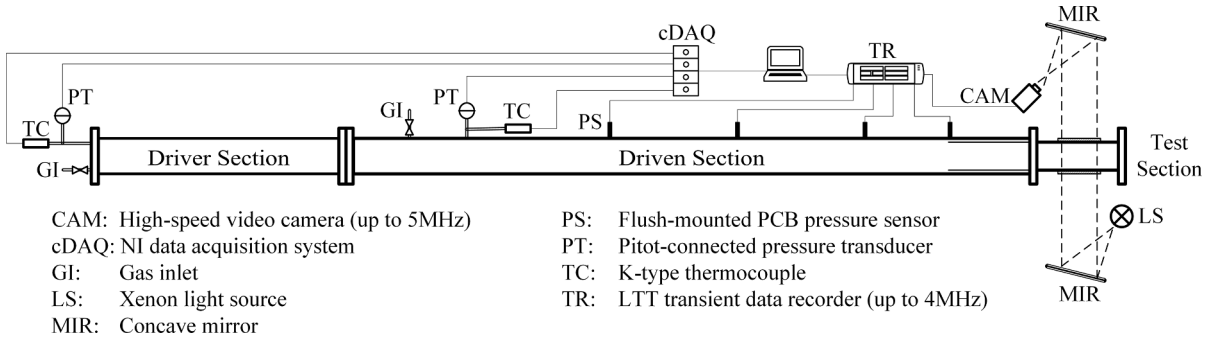

Fig. 2-1. Sketch of the shock tube and connected systems that were used for bubble experiments.

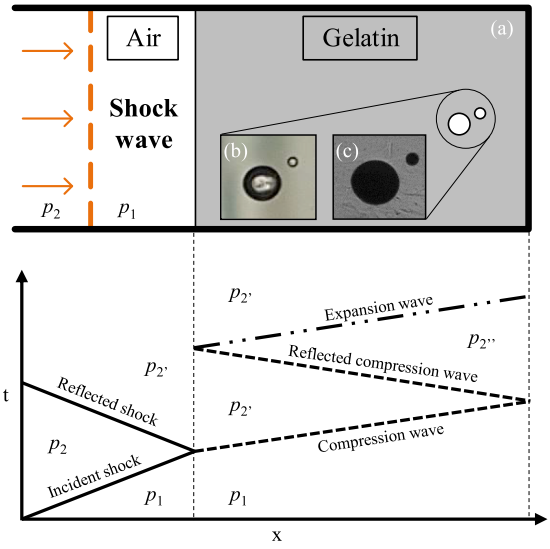

Fig. 2-2. Sketch of the test section filled with gelatin (a). Two bubbles in gelatin are depicted as a direct photograph (b) and as a shadowgraph image (c). The wave motion and pressure change during the experiment is presented in a wave diagram.

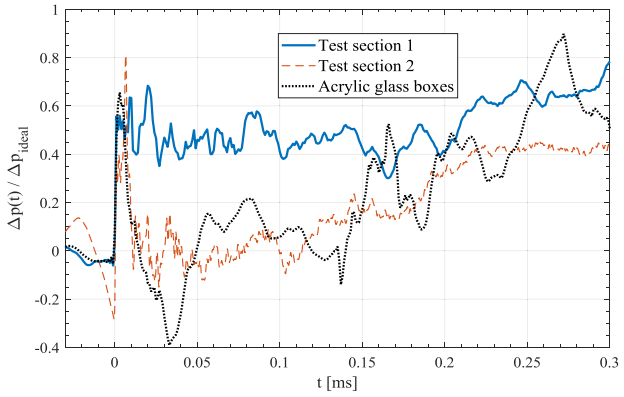

Fig. 2-3. Comparison of the pressure signal at the back wall of test section 1, test section 2, and of the acrylic glass box.

shock speed in front of the test section. Typically, three sensors monitored the pressure in the gelatin at the side of the test section and one sensor at the back wall of the test section.

2.2. Influence of the test section

To conduct the experiments, three different types of setups were available:

- Acrylic glass box: a box, made of 10 mm thick acrylic glass plates that was placed inside the test sections and exposed to the shock wave.
- Test section 1 (TS1): A test section formed out of a solid aluminum alloy cylinder with a wall thickness of up to 130 mm.
- Test section 2 (TS2): A multi-purpose test section that featured side walls made of 40 mm thick aluminum alloy plates.

One main objective of the experiments is to establish a high and constant surrounding pressure after a short rise time to initiate the bubble collapse. However, rise time and evolution of the pressure were strongly dependent on the applied setup. Fig. 2-3 shows the transient pressure signals at the back wall for all three cases. The measured pressure change $\Delta p(t) = p(t) - p_1$ is normalized by the expected ideal pressure change after the reflected compression wave Δp_{ideal}. The figure shows an instantaneous pressure rise in all three signals after the arrival of the compression wave. Apart from this instantaneous rise, the ideal one-dimensional wave motion with constant post shock conditions is poorly reproduced and the expected pressure value $\Delta p(t)/\Delta p_{ideal} = 1$ is not reached. In addition, only the pressure in TS1 stays at a comparatively constant high level, whereas the pressure drops rapidly after the initial peak in the other cases. The short pressure peaks for the acrylic glass box and TS 2 are insufficient in this setup to initiate the bubble collapse and neither is the sustainable but slow pressure rise that occurs after more than 0.1 ms. However, good results were achieved with TS1. The pressure signal shows a significant increase and a constant value within the range of $0.4 < \Delta p(t)/\Delta p_{ideal} < 0.6$. Bubbles react to the fast rise time and the constant, high driving pressure and collapse strongly. Consequently, TS1 was used for all experiments that are presented in this work.

The reason for the untypical pressure signals was found to be the deformation of the structure that surrounds the liquid. A high pressure in the test section is reached behind the compression wave. This applies a strong load on the solid structure, which reacts by outward deformation. Since water, or gelatin in this case, is an almost incompressible liquid, a small expansion results in an immediate and strong decrease of pressure. Overall, the pressure only increases slowly, which prevents the bubbles from collapsing strongly. While a deformation of the acrylic glass box was expected, a relevant deformation of metal came as a surprise.

However, at this point the authors would like to point out that the value Δp_{ideal}, cannot be achieved even with infinitely thick sidewalls. Taking the compressibility of the metal back wall into account, a part of the shock is transmitted into the metal and the maximum pressure rise Δp_{max} can be calculated from one-dimensional acoustic theory (e.g. Brekhovskikh [31]) by

$$\Delta p_{max} = \frac{1 + R}{2} \Delta p_{ideal} \quad (2)$$

with

$$R = \frac{\rho_{Al} a_{Al} - \rho_W a_W}{\rho_{Al} a_{Al} + \rho_W a_W}. \tag{3}$$

Taking the speed of sound a and the density ρ of water and aluminum, this results in $\Delta p_{max} \approx 0.9\ \Delta p_{ideal}$. The estimation can be extended from a 1D to a 3D problem, by taking the compressibility of the side walls into account. Doing this, the value is expected to be even lower. Consequently, the actual pressure rise is strongly limited in all experimental works that apply similar setups. For the present work, it results in a pressure signal that is not perfect but provides a sharp pressure jump followed by a high-pressure plateau.

3. Influence of the gelatin

Gelatinous fluids are used occasionally to study bubble dynamics. Dear et al. [26,32] produce arrays of two-dimensional cavities in gelatin and induce the collapse with a strong shock wave to investigate the liquid jet development. A similar setup is employed by Bourne and Field [33,34] to study the collapse of differently shaped cavities and the associated luminescence. Another work by Swantek and Austin [27] examines the interaction of voids in gel with a stress wave and measures the surrounding velocity field. For such experiments and the corresponding high pressures, it is usually stated that the gelatin behaves as a liquid (e.g. [32]). The shear-thinning property of the gelatin may affect bubble dynamics, especially in the present study with only moderate pressure levels of less than 1 MPa. Therefore, we compare the results using gelatin with the standard case of bubbles in water. Different gelatin mixtures are used and compared at different pressure levels.

3.1. Rayleigh-Plesset equation

A well-known formula, often serving as the standard reference to describe spherical cavitation bubbles, is the Rayleigh-Plesset equation. We use the general form of the equation after Brennen [3] but modify it to describe bubbles filled with non-condensable gas. We expect that only air at atmospheric pressure is present at the collapse initiation. Furthermore, we assume that the gas compresses and expands adiabatically, i.e. without heat transfer between bubble and surrounding liquid. The time-dependent gas pressure $p_G(t)$ within the bubble can then be written as [3]:

$$p_G = p_{G0}\left(\frac{R_0}{R}\right)^{3\kappa} \tag{4}$$

with p_{G0} as the initial pressure in the gas bubble, R_0 as the initial radius and R as the time-dependent radius of the bubble. The mentioned assumptions result in the modified equation

$$\frac{p_{G0}\left(\frac{R_0}{R}\right)^{3\kappa} - p_\infty(t)}{\rho_L} = R\frac{\mathrm{d}^2R}{\mathrm{d}t^2} + \frac{3}{2}\left(\frac{\mathrm{d}R}{\mathrm{d}t}\right)^2 + \frac{4\upsilon_L}{R}\frac{\mathrm{d}R}{\mathrm{d}t} + \frac{2S}{\rho_L R} \tag{5}$$

with t as the time, $p_\infty(t)$ as the pressure in the fluid, ρ_L and υ_L as the density and kinematic viscosity of the liquid respectively and S as the surface tension of the liquid. Along with the measured initial radius from the images and the recorded pressure $p(t)$ at the end wall, this formula provides a valuable tool. It allows to calculate a reference for each experiment individually. The properties of water are taken to describe the liquid to further assure a general and well-known reference. Comparing results of the theory with experiments can show differences and thus the influence of the gelatin.

3.2. Experiments

The influence of the gelatin on the bubble collapse was evaluated for Gelrite™ concentrations between 0.42 and 0.96 g/l mixed with 0.35–0.8 g/l $MgSO_4$, respectively. Table 3-1 presents an overview of the tested mixtures. Mixture 1 represents a lower limit below which bubbles start to rise. Mixture 4 represents an upper limit for which the gelatin is very solid, and bubbles tend to be of an aspherical shape. To allow additional insight, experiments with the four mixtures were conducted at different pressures. The pressure rise $\bar{\Delta p}$, averaged over the collapse time, reached values between $\bar{\Delta p} = 0.36$ bar as a lower limit and up to $\bar{\Delta p} = 3.38$ bar as a higher limit.

Table 3-1
Test matrix to evaluate gelatin influence, providing the respective Gelrite and $MgSO_4$ concentrations as $c_{Gelrite}$ and c_{MgSO4}, a ratio to the standard case c_2 and the number of conducted experiments n_{exp}.

Mixture	$c_{Gelrite}$ [g/l]	c_{MgSO4} [g/l]	c/c_2	n_{exp}
1	0.42	0.35	70%	9
2	0.6	0.5	100%	14
3	0.78	0.65	130%	5
4	0.96	0.8	160%	14

3.2.1. High-speed imaging

Essential qualitative features of the bubble oscillation are presented with exemplary photographic sequences. Note that for all presented images, the compression wave arrives from the left but is reflected at the back wall, which is to the right of the images but out of the view. Fig. 3-1 shows bubble compression and expansion for a high-pressure increase of $\bar{\Delta p} = 2.82$–3.38 bar for different gelatin mixtures. Fig. 3-1(a) shows the oscillation for gelatin of mixture 1 and a bubble of $R_0 = 1.27$ mm. The gelatin is very clear, and the bubble shape appears perfectly spherical. After the passage of the compression wave, the bubble starts to contract spherically (frames 1–6) until it reaches a minimum value (frame 7). The spherical shape is disturbed along the equator of the bubble during the rebound (frames 8–14). An extrusion develops and stays pronounced, while the shape stays symmetric otherwise. The bubble collapses and rebounds a second time in the following frames. Here, the shape changes significantly and the bubble shows aspherical behavior.

Fig. 3-1(b) shows results with mixture 2. The bubble of $R_0 = 1.28$ mm is of almost spherical shape, but surrounding gelatin is not completely clear due to scattered dirt particles. Comparable to the previous case, the bubble remains spherical during the collapse (frames 1–7) and develops a small extrusion along the equator at the beginning of the rebound (frame 8). This deformation remains visible during the rebound (frames 9–14) and the second collapse (frames 15–19). Again, the bubble starts to deform stronger during the second oscillation.

Different phenomena can be observed, when the Gelrite™ concentration is further increased. A bubble of $R_0 = 1.23$ mm, placed in gelatin of mixture 3, is presented in Fig. 3-1(c). The initial shape is not completely spherical but slightly elongated horizontally. In addition, the gelatin shows a non-uniform structure at the bottom of the images. Nevertheless, the dynamic response is similar as before with a uniform collapse (frames 1–7), a slightly deformed rebound (frames 8–13) and an enhanced deformation afterwards (frames 14–20).

Fig. 3-1(d) shows an experiment with mixture 4, the densest gelatin. The figure shows a bubble with an initial radius of $R_0 = 1.42$ mm that appears slightly deformed. As in the previous case, a structure in the gelatin is visible around the bottom half of the bubble. The bubble initially collapses uniformly (frames 1–8) but develops an indentation on the left side during the rebound (frames 9–16). The larger size and the lower driving pressure of that case prolong the collapse and the rebound phase.

One example for a collapse under a lower pressure is presented in Fig. 3-2. The sequence shows a very spherical bubble of $R_0 = 1.27$ mm in a gelatin of mixture 2. After the pressure increase follows an oscillating motion with a contraction (frames 1–11) and an expansion (frames 12–20). In contrast to the previously shown experiments, only a

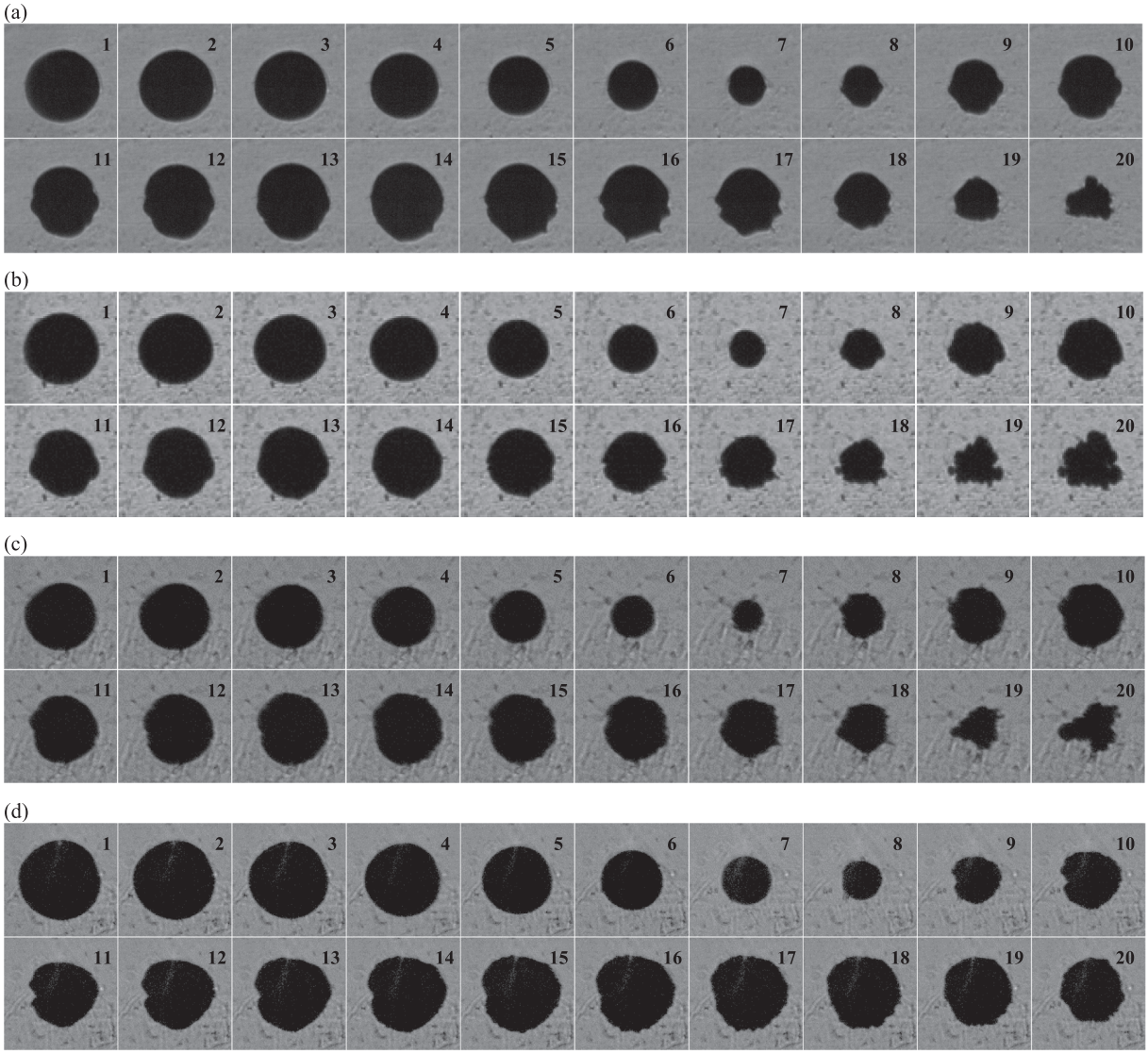

Fig. 3-1. Oscillation of air bubbles in gelatins of different mixtures. The frame size is 4.0 × 4.0 mm^2 and the interframe time is 12 µs. (a) mixture 1 (70% c_2), R_0 = 1.27 mm, $\bar{\Delta p}$ = 3.25 bar; (b) mixture 2 (standard mixture), R_0 = 1.28 mm, $\bar{\Delta p}$ = 3.26 bar; (c) mixture 3 (130% c_2), R_0 = 1.23 mm, $\bar{\Delta p}$ = 3.38 bar; (d) mixture 4 (160% c_2), R_0 = 1.42 mm, $\bar{\Delta p}$ = 2.82 bar.

weak oscillation amplitude is observed, and the bubble always stays in a very spherical shape. We omit here image sequences for other mixtures, as they show a similar weak, and spherical oscillation.

3.2.2. Radius data

To allow a quantitative analysis, we deduce a time-dependent equivalent bubble radius from all image sequences. Pixels that are part of the bubble were counted and a pixel size was provided with a reference length. An area A was calculated, and the equivalent radius R was taken as $R = (A/\pi)^{0.5}$. This method is exact only for bubbles of perfect sphericity, but it also provides a good representation for bubbles that are only slightly deformed.

As an example, Fig. 3-3 shows the equivalent radius along with the calculated reference for the experiment that was shown in Fig. 3-1(a). The reference calculation is based on Eq. (5) and uses the measured pressure $p(t)$ as an input. The result is plotted as a solid blue line while data points for each of the 128 frames of the captured video are depicted as black crosses. An initial time of $t = 0$ is assigned to the first

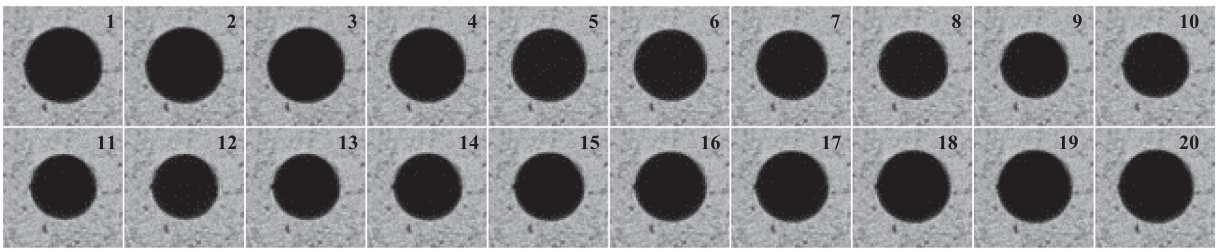

Fig. 3-2. Oscillation of an air bubble in gelatin of mixture 2 (standard mixture) after a low-pressure increase ($\bar{\Delta p}$ = 0.44 bar). The interframe time is 16 µs, the frame size 4.00 × 4.00 mm^2 and the initial radius is R_0 = 1.27 mm.

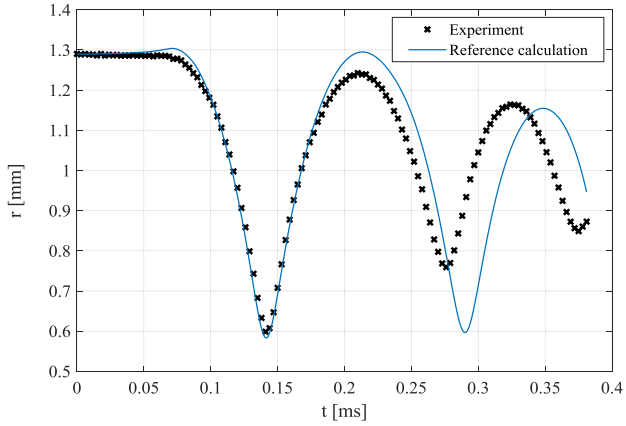

Fig. 3-3. Time-dependent equivalent radius for a single bubble in gelatin of mixture 2 under a high pressure. The corresponding image sequence is displayed in Fig. 3-1 (b). The reference calculation uses the presented Rayleigh-Plesset equation with the case-specific pressure signal $p(t)$ and the properties of water for the liquid.

frame, while the pressure increase that starts the oscillation occurs later. There is a good agreement between the two curves during the first collapse and rebound. For both curves the value and the time of the minimum radius match almost perfectly. Notably, the calculation initially shows a small increase of the radius. This increase reflects the pressure drop before the arrival of the compression wave (compare Fig. 2-3), whereas no visibly growth was detected for this experiment. After the first oscillation, the two curves show a different behavior. The experimental result shows a lower oscillation amplitude at a higher frequency. Both effects are even more pronounced during the following motion until the recording of the video ends.

A comparable behavior, from a qualitative point of view, is visible for experiments at a lower pressure. Fig. 3-4 shows the radius data that corresponds to the experiment presented in Fig. 3-2. The oscillation is much slower and of a much lower amplitude than for higher pressures, but still exhibits the same overall behavior. The curves match very well during the initial phase and during the beginning of the collapse. Towards the end, the curves deviate and the experimentally observed bubble oscillation in gelatin is dampened stronger than the calculated reference in water.

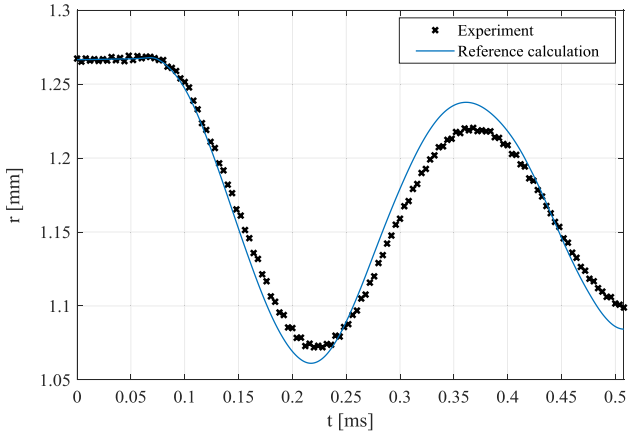

Fig. 3-4. Time-dependent equivalent radius for a single bubble in gelatin of mixture 2 under a lower pressure. The corresponding image sequence is displayed in Fig. 3-2. The reference calculation uses the presented Rayleigh-Plesset equation with the case-specific pressure signal $p(t)$ and the properties of water for the liquid.

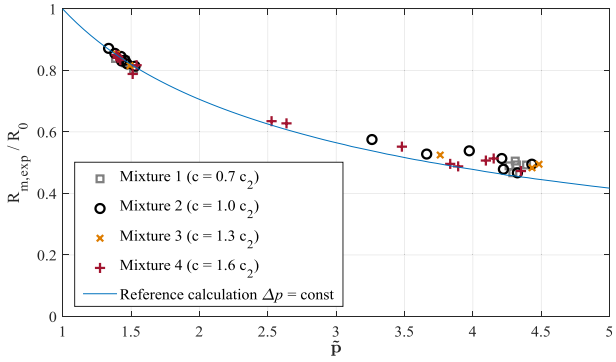

Fig. 3-5. Minimum radius $R_{m,exp}$, normalized by the initial radius R_0 in dependency of the normalized driving pressure during the collapse phase $\tilde{p}$. Different gelatin mixtures are highlighted according to the legend.

3.2.3. Non-dimensional parameters

Several non-dimensional parameters can be deduced from the radius data to describe the collapse behavior. A first overview is shown in Fig. 3-5 and presents the ratio between the minimum radius $R_{m,exp}$ and the initial radius R_0 for each experiment over a normalized driving pressure $\tilde{p}$. Here, $\tilde{p}$ is calculated as the ratio between the average pressure during the collapse $\bar{p}_c$ and the initial pressure in the driven section p_1. Different gelatin concentrations are indicated by different symbols according to the legend. In addition, a reference calculation is plotted that, in this case, uses a constant Δp as the input for the calculation. The figure shows that a smaller radius is reached for an increasing driving pressure. The slope of this trend is steep at the beginning but starts to flatten out at a higher pressure. In general, the experimental results are very close to the theory. At a higher pressure, a difference starts to appear, and the experimental data indicates higher values of the ratio than the theory. Although indicated in the figure, different Gelrite™ concentrations do not show a different behavior.

To investigate the behavior in more detail, we can normalize each experiment with the corresponding calculation. The normalized minimum radius, R^*, is then defined as

$$R^* = \frac{R_{m,exp}}{R_{m,RP}} \tag{6}$$

with $R_{m,RP}$ as the minimum radius from the case-specific calculation with the Rayleigh-Plesset equation. In addition, we calculate a collapse time to provide a temporal reference. The collapse time is defined as the time from the arrival of the compression wave at the bubble position until the moment when the minimum radius is reached. The collapse time of the experiment $t_{c,exp}$ is normalized by the collapse time of the reference calculation $t_{c,RP}$ to give

$$t^* = \frac{t_{c,exp}}{t_{c,RP}}. \tag{7}$$

Fig. 3-6 gives an overview of R^* plotted with respect to $\tilde{p}$. Due to the normalization, the differences appear enhanced. The experimental results match the calculated reference value very accurately for a low-pressure increase. All data points are in a range between $R^* = 0.99$ and $R^* = 1.015$. For increasing pressure, the figure shows a wider range of R^* with data points spread out at a higher level of $R^* = 1$–1.15. Again, the data points for different gelatin concentrations do not show any tendencies but appear randomly distributed.

The corresponding overview for the collapse time is presented in Fig. 3-7. In contrast to the previous case, the data points are not only spread around for the higher, but also for the lower pressure. The value of t^* ranges between $t^* = 0.91$ and $t^* = 1.11$ and data points are well-distributed in between. Calculating the average gives a value of $t^* = 1.01$, which verifies the general similarity to water. However, the evaluation of the impact of the gelatin concentration is difficult since a

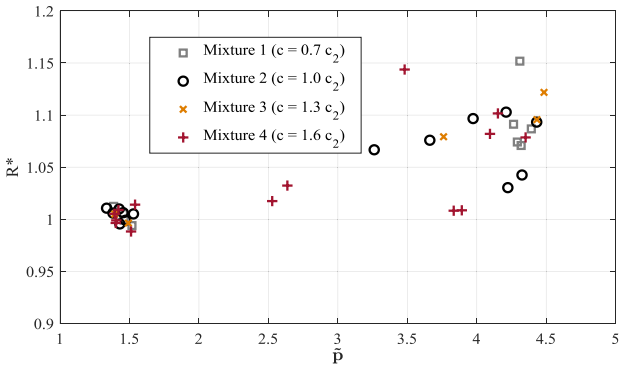

Fig. 3-6. Normalized minimum radius R^* plotted in dependency of the normalized driving pressure during the collapse phase $\tilde{p}$. Different gelatin mixtures are highlighted according to the legend.

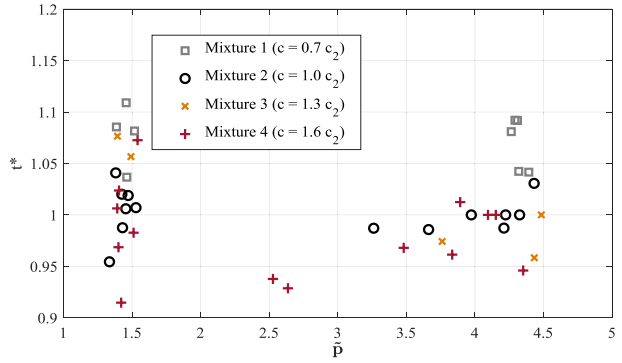

Fig. 3-7. Normalized collapse time t^* plotted in dependency of the normalized driving pressure during the collapse phase $\tilde{p}$. Different gelatin mixtures are highlighted according to the legend.

clear statement is not possible. At first glance, it looks like increasing the gelatin concentration leads to decreased collapse times. But some data points clearly contradict this impression. Thus, we expect that this is an effect of general uncertainty and the limited number of experiments. Especially, no corresponding effect is observed with respect to R^*, and comparable work with cavitation bubbles shows that adding polymer additives to water for non-Newtonian behavior does not significantly affect the growth and collapse of a bubble [35,36].

3.3. Discussion

3.3.1. A comment on the accuracy

Before assessing the bubble behavior in detail, it is worth highlighting some uncertainties and inaccuracies of the presented method.

- Resolution: The experimental setup limits the accuracy of the optical measurement data. Both a spatial and a temporal limit results directly from the camera system. Typically, the bubble is resolved at a resolution of 30–63 µm pixel^{-1} with around 40–80 pixels per diameter. This results in a spatial inaccuracy for the radii of $\Delta r = \pm 1.25$–2.5% when assuming an error within one pixel. The temporal evolution of the collapse is typically captured between 20 and 40 images, which gives a temporal inaccuracy for the collapse time of $\Delta t_c = \pm 1.25$–2.5% when considering an error of half the interframe time.
- Minimum radius: The temporal inaccuracy includes an additional drawback onto the spatial error. Due to the limited number of frames, it cannot be assured that the minimum radius is always captured. This directly results in a systematic error that overestimates the minimum radius. The error depends on the curvature of $r(t)$ close to the minimum. For example, the minimum radius $r_{m,exp}$ is overestimated up to $\Delta r = 0.77\%$ for the experiment presented in Fig. 3-3 and up to $\Delta r = 0.016\%$ for the experiment of Fig. 3-4.
- Bubble shape: The application of gelatin in this setup leads to inhomogeneities in the liquid surrounding the bubble, whether through a non-uniform cool-down or the insertion of the needle for bubble production. These disturbances affect the symmetry of the bubble collapse and introduce an error when calculating the equivalent radius. Special care was taken to maximize the level of sphericity of the initial bubble and minimize deformation during the oscillation. To account for a potential deformation in the direction normal to the image plane, we inspected the bubbles carefully before the experiments. Nevertheless, some uncertainty with respect to the bubble shape remains and is difficult to assess.

3.3.2. Assessment of the gelatin influence

One main aspect of this study was to compare the behavior of the bubbles in gelatin with the reference case of bubbles in water. Overall, it was shown that bubbles in both cases behave similarly, especially during the first collapse. Representative image sequences show that bubbles initially collapse in a spherical shape, and the corresponding radius plots agree well with the theory (see Figs. 3-3 and 3-4). Furthermore, non-dimensional parameters shown in Figs. 3-5–3-7 confirm the overall similarity, but also highlight some differences. Overall, two main aspects stand out.

- Despite qualitatively very different gelatin mixtures, the results show that the gelatin concentration does not influence the bubble behavior noticeably. This indicates that non-Newtonian properties play a minor role. Although it is difficult to compare to previous work, this result agrees with other research on non-Newtonian liquids. Brujan and Williams [35] investigate for example the effect of polymer additives on cavitation bubbles and note that no different behavior is noticed when bubbles of a radius larger than 0.5 mm are studied. Further support stems from measurements of fluid properties. Deasy et al. [37] provide a yield (shear) stress of 1150 Pa for a Gelrite™ mixture similar to mixture 2. This value is small compared to the driving pressure levels of 0.36–3.38 bar, which supports the reduced influence.
- At lower driving pressures, the bubbles in gelatin behave similarly to water. Applying a higher driving pressure leads to larger deviations between experiment and theory with respect to the minimum radius (Figs. 3-5 and 3-6). As afore mentioned, non-Newtonian behavior is expected to be minor, but the discrepancy can be explained by the aspherical behavior of the bubble during the collapse. Deformation is enhanced for higher driving pressures and often starts to appear when the minimum radius is reached. For example, often a deformation along the equator of the bubble appears directly after the first collapse (compare Fig. 3-1(a–b)). This makes it difficult to identify the minimum radius accurately and in general leads to an overestimation of the calculated equivalent radius, which explains the observed trend.

The presented conclusions apply for the first collapse, while subsequent oscillations differ significantly from the performed reference calculation. Besides the mentioned increased asymmetry of the bubble in time, the higher viscosity of the gelatin lowers the oscillation amplitude and affects the oscillation frequency.

In summary, the shown cases demonstrate that gelatin is a suitable surrogate for water and can be utilized for studies of bubble dynamics that focus on the initial bubble collapse. Care must be taken to assure a spherical bubble shape, but the obtained results for collapse time and minimum radius show no dependency with respect to the gelatin concentration.

4. Bubble pairs

A conclusion of the previous section is that limitations of the setup do not limit the possibility to conduct research on a more general level. Thus, we use the experimental setup to produce multiple bubbles and study the interaction of gas bubble pairs.

4.1. Non-dimensional parameters

Typically, three non-dimensional parameters are defined to characterize bubble pairs: a relative distance, a size ratio and a phase difference. Chew et al. [38] define the relative initial bubble distance as

$$\gamma = \frac{d}{R_1 + R_2} \tag{8}$$

where d is the distance between the bubble centers and R_1 and R_2 are the maximum radii of the two interacting bubbles. Furthermore, the size difference is defined as

$$S = \frac{R_L}{R_S} \tag{9}$$

with R_L and R_S as the maximum radius of the large and the small bubble respectively. The third parameter, $\Delta\theta$, indicates the phase difference of the two bubbles, but the definition in the literature cannot be easily applied here, due to the different experimental setups. Experiments in related literature produce vapor cavities by means of laser-focus or electric discharge, while in this study, gas bubbles are present in an initially stationary setup. This leads, for example, to the problem that no well-defined time difference Δt of bubble initiation exists. Thus, the definition of Chew et al. [38]

$$\Delta\theta = \left| \left(\frac{t_1}{t_{osc,1}} - \frac{t_2}{t_{osc,2}} \right) \right| + \frac{\Delta t}{t_{osc,1}} \tag{10}$$

simplifies for the current case to

$$\Delta\theta = \left| \left(\frac{t_{osc,1}}{t_{osc,1}} - \frac{t_{osc,1}}{t_{osc,2}} \right) \right| = 1 - \frac{t_{osc,S}}{t_{osc,L}} \tag{11}$$

where t_{osc} gives an oscillation period, taken here as the time from maximum to minimum bubble radius in contrast to the duration from bubble nucleation to bubble collapse in the original definition. With the oscillation time of the smaller bubble, $t_{osc,S}$, being shorter than the oscillation time of the bigger bubble, $t_{osc,L}$, always a positive value for the phase difference results. Consequently, a value of $\Delta\theta = 0$ results as the minimum for equally sized and equally oscillating bubbles. A value of $\Delta\theta$ close to 1 represents bubbles of largely different sizes. Han et al. [39] note that $\Delta\theta$, in its original definition, is not independent of S. Instead, they propose a different parameter, τ, as a relative initiation time difference. Applied to the present setup, this parameter would always give a value of $\tau = 0$, as bubbles are initially present. However, following their initial reasoning, we can assume a linear relation between radius and collapse time that can be justified by the Rayleigh collapse time for single bubbles [3]. This results in the phase difference solely depending on the size ratio, and Eq. (11) transforming to:

$$\Delta\theta = 1 - \frac{R_S}{R_L} = 1 - \frac{1}{S} \tag{12}$$

It should be noted, that the normalized distance γ is calculated from the two-dimensional image, so the value is only accurate if the centers of the two bubbles are in the same plane normal to the light path. The distance can be underestimated if one bubble is displaced along the light path.

4.2. Types of interaction

The behavior of bubble pairs was investigated for differently sized bubbles of $S = 1.0$–7.36 ($\Delta\theta = 0.0$–0.87) at various distances of $\gamma = 0.99$–1.97. All experiments were conducted in the high-pressure range and, except for two cases, only gelatin of mixture 2 was used. In general, the bubble interaction can be observed clearly during the first oscillation, whereas bubbles often show an irregular shape after the second collapse. This is in accordance to results of the previous section. In addition, liquid jets are not observed directly in the presented image sequences, but there are clear indications for them. Identifying the jets serves as a main feature to separate different bubble behavior and helps to define four types of bubble pair interaction that are presented in the following.

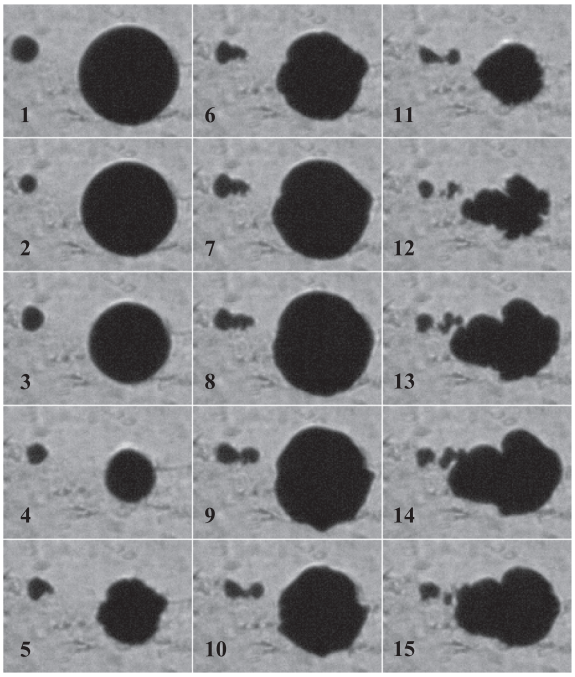

Fig. 4-1. Interacting bubble pair with $R_L = 1.0$, $R_S = 0.26$, $S = 3.86$, $\Delta\theta = 0.74$ and $\gamma = 1.74$. The interframe time is 16 µs.

4.2.1. Weak interaction

The first type describes a bubble pair that does not interact strongly due to the large size ratio and relative distance. Fig. 4-1 presents a corresponding example with a big bubble and a small bubble ($S = 3.86$) that are a certain distance apart ($\gamma = 1.74$). The small bubble on the left collapses immediately after the pressure increase (frame 2) and oscillates at a high frequency. It follows the motion of the collapse of the big bubble (frames 1–4) and starts to elongate once the big bubble rebounds (frames 5–8). As soon as the big bubble contracts again, the small bubble follows this movement, whereas the big bubble seems not affected by any interaction. Consecutive frames show that the small bubble starts to split into two parts (frames 9–12). A tiny bubble fragment remains, but the closer part eventually is captured by the big bubble that now has a very aspherical shape (frame 15). For this case, the general dynamics is dominated by the big bubble. It creates a periodic movement that, combined with the high-frequency oscillation of the small bubble, leads to bubble splitting.

4.2.2. Shooting through

For small bubbles that are close to the main bubble, we observe a 'shooting through' behavior. Fig. 4-2, shows an image sequence with a similar size ratio as the previous case ($S = 4.08$), but now with the two bubbles close together ($\gamma = 0.99$). After the pressure increase, the big bubble collapses spherically (frames 1–6), while the small bubble contracts and follows the boundary of the big bubble. The two bubbles merge (frame 4) and the remaining bubble maintains a spherical shape

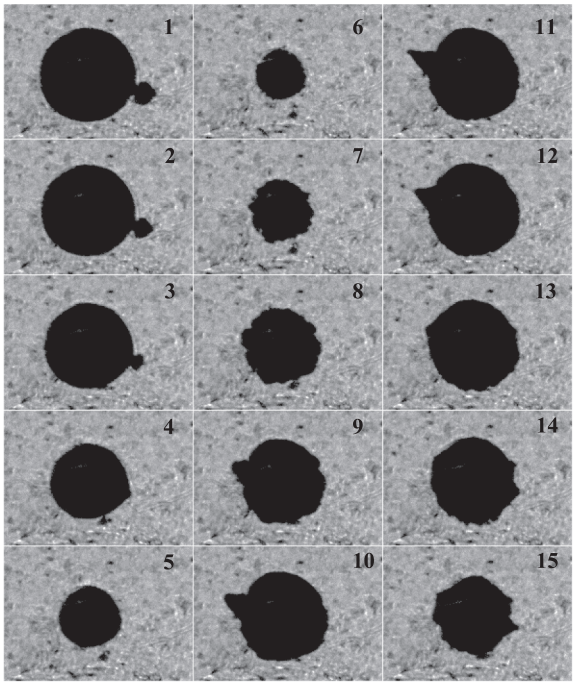

Fig. 4-2. Interacting bubble pair with $R_L = 1.51$, $R_S = 0.37$, $S = 4.08$, $\Delta\theta = 0.76$ and $\gamma = 0.99$. The interframe time is 16 µs.

during the collapse and initial rebound. However, the collapse of the small bubble into the big bubble induces a liquid jet that shoots through the big bubble and penetrates the surface on the far side during the rebound. The effect is seen as a funnel-shaped protrusion that develops at the side opposite to the original position of the small bubble (frames 9–13). This type of behavior is, as such, not presented in the literature, but setting up bubbles in this constellation provides an opportunity to generate a controlled and directed liquid jet.

4.2.3. Reversing collapse

A reversing collapse is observed for the combination of a large and a medium-sized bubble. An example of this case is presented in Fig. 4-3 with $S = 1.71$ and $\gamma = 1.24$. Both bubbles contract spherically in the initial phase (frames 1–3), but the medium-sized bubble collapses faster due to the smaller size. This collapse is aspherical and creates a jet on

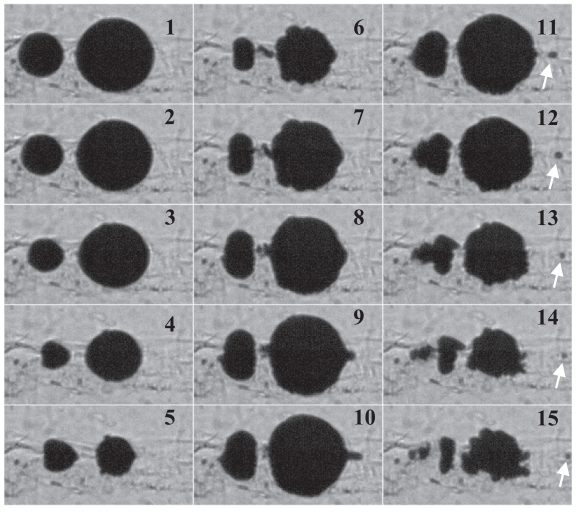

Fig. 4-3. Interacting bubble pair with $R_L = 1.09$, $R_S = 0.63$, $S = 1.71$, $\Delta\theta = 0.42$ and $\gamma = 1.24$. The interframe time is 16 µs. White arrows highlight a small bubble that detaches from the main bubble.

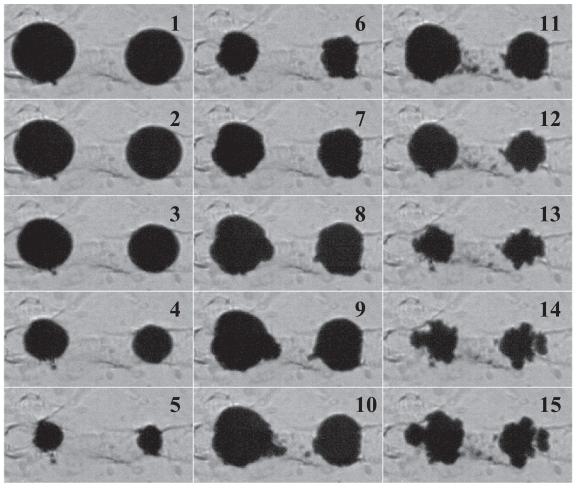

Fig. 4-4. Interacting bubble pair with $R_L = 0.91$, $R_S = 0.84$, $S = 1.09$, $\Delta\theta = 0.08$ and $\gamma = 1.86$. The interframe time is 12 µs.

the right side towards the other bubble (frame 5–6). A part of this jet quickly disconnects from the bubble and remnants remain visible in between the two bubbles. After this collapse, the motion reverses and the medium-sized bubble expands in the opposite direction (frames 7–10). The medium-sized bubble first shows a shape that points away from the big bubble (frames 11–12) and then splits into two parts (frames 13–15). Meanwhile, the large bubble behaves similarly to the previous case and again shows a jet away from the smaller bubble. A small satellite bubble detaches from that jet and continues to move to the right (frames 11–15, highlighted by white arrows). The aspect of both bubbles jetting away from each other provides some similarities to previous work. Chew et al. [38] simply define one interaction type as 'jet away'. However, the reversing motion also indicates some differences and in some way shows more similarities to what Chew et al. [38] label the 'catapult' type and Han et al. [39] describe as anti-phase bubble pairs.

4.2.4. Collapse towards

A final type describes bubbles that collapse towards each other. For the presented example in Fig. 4-4, the bubbles are of similar size ($S = 1.09$) and farther apart ($\gamma = 1.86$). Both bubbles collapse spherically (frames 1–5) but show an aspherical behavior during the rebound. They develop a liquid jet directed to the other bubble that is visible as a protrusion (frames 8–10). The bubble motion is largely in phase and often appears symmetric. The following oscillation still shows a directional behavior that slowly brings the bubbles closer together. This behavior is well known and has also been shown more recently in other experimental work [7,29,39].

4.3. Characterization with non-dimensional parameters

Having classified different types of bubble interaction we can display the type for each conducted experiment with respect to $\Delta\theta$ and γ (Fig. 4-5). Three experiments are characterized as in between, because they show a mixed behavior with aspects of two other types.

The figure shows that the same interaction behavior is associated to distinct regions of $\Delta\theta$ and γ. This indicates that there is a relation between the non-dimensional parameters and the interaction type. This would allow a prediction of the bubble behavior that solely depends on the initial configuration of the bubble pair. It is difficult to compare these results to previous findings in the literature due to the different experimental setup, but Chew et al. [38] apply a similar classification with respect to $\Delta\theta$ and γ for their experiments. For $1 < \gamma < 2$ their work identifies two distinct regions of different behavior as 'jet towards' and 'jet away'. The regions are separated by a critical phase difference

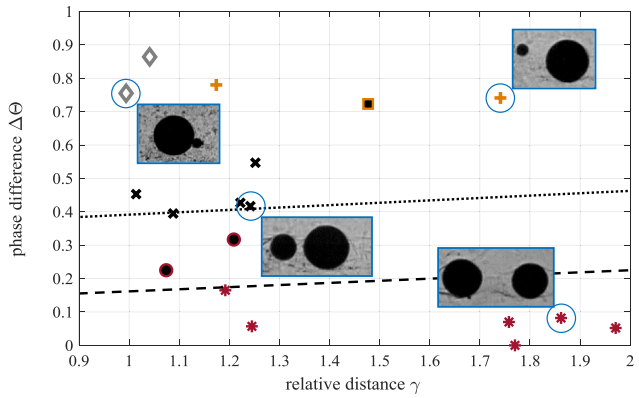

Fig. 4-5. Types of bubble pair interaction with respect to $\Delta\theta$ and γ: Weak interaction (orange plus icon), shooting through (gray diamond), reversing collapse (black cross), collapse towards (red star), and mixed type behavior (black dot in red circle and black square surrounded by an orange line). The dashed and dotted lines present, for reference, the critical $\Delta\theta_c$ value after Chew et al. [38] that separates the types of 'jet away' ($\Delta\theta > \Delta\theta_c$) and 'jet towards' ($\Delta\theta < \Delta\theta_c$) for bubbles of similar and different size respectively. (For interpretation of the references to color in this figure legend, the reader is referred to the web version of this article.)

$\Delta\theta_c$ that is around 0.2 for similarly-sized bubbles (dashed line) and around 0.45 for differently-sized bubbles (dotted line). Bubbles collapse towards each other when $\Delta\theta$ is below the critical value, and away from each other when a $\Delta\theta$ higher than the critical value. This behavior agrees well with the separation in Fig. 4-5 between the type of collapse towards and of reversing collapse. Chew et al. [38] also define two other distinct regions of the types coalescence and catapult, but they are located at $\gamma < 1$. Such a value cannot be reproduced in the present study. In contrast, the interaction of a very small bubble with a larger bubble is only discussed in the present work and is not mentioned specifically in the literature.

5. Conclusion

In this work, we present a new type of experimental setup and discuss its advantages and limitations. In a first part, the setup is used to investigate the influence of gelatin on bubble dynamics. Results show that bubbles in gelatin behave very similarly to bubbles in water during the first oscillation and that changing the gelatin concentration does not have a noticeable influence on the bubble collapse. In a second part, we study the interaction of gas bubble pairs in the free field and find four types of bubble pair interaction that can be defined by non-dimensional parameters. This classification differs from the literature in some respects due to the use of pure gas bubbles instead of vapor bubbles.

The results of this work indicate the potential of the setup, but also show some limitations. One remaining challenge is the production of a uniform gelatin and a perfectly spherical bubble. In addition, further improvements in the optical system can help to reduce the uncertainty and provide deeper insight into the collapse behavior. Future investigations can take advantage of these improvements and of the possibilities of the setup. An interesting option is to create bubbles of different gas content and study the effect on the bubble behavior or to study the interaction of a collapsing bubble with soft material. However, more work on bubble-bubble interaction should also be aimed for to study a wider range of S and γ or possibly expand from bubble pairs to several interacting bubbles.

Declaration of Competing Interest

There is no financial or personal relationship between authors and other people or organizations that could inappropriately influence or bias the work.

Acknowledgements

The authors acknowledge funding by the European Research Council (ERC) under the European Union's Horizon 2020 research and innovation program (grant agreement No. 667483).

References

[1] Z. Wang, T. Hopfes, M. Giglmaier, N.A. Adams, Influence of non-Newtonian gelatinous fluids on bubble collapse dynamics, 5th Int. Conf. Exp. Fluid Mech. (2018).
[2] T. Hopfes, Z. Wang, M. Giglmaier, N.A. Adams, Dynamics of collapsing multi-bubble arrangements, 5th Int. Conf. Exp. Fluid Mech. (2018).
[3] C.E. Brennen, Fundamentals of Multiphase Flow, Cambridge University Press, Cambridge, 2005https://doi.org/10.1017/CBO9780511807169.
[4] C. Chaussy, W. Brendel, E. Schmiedt, Extracorporeally induced destruction of kidney stones by shock waves, Lancet (London, England). 2 (1980) 1265–1268.
[5] A.J. Coleman, J.E. Saunders, A review of the physical properties and biological effects of the high amplitude acoustic fields used in extracorporeal lithotripsy, Ultrasonics 31 (1993) 75–89, https://doi.org/10.1016/0041-624X(93)90037-Z.
[6] E. Unger, T. Porter, J. Lindner, P. Grayburn, Cardiovascular drug delivery with ultrasound and microbubbles, Adv. Drug Deliv. Rev. 72 (2014) 110–126, https://doi.org/10.1016/j.addr.2014.01.012.
[7] S.W. Fong, D. Adhikari, E. Klaseboer, B.C. Khoo, Interactions of multiple spark-generated bubbles with phase differences, Exp. Fluids 46 (2009) 705–724, https://doi.org/10.1007/s00348-008-0603-4.
[8] O. Lindau, W. Lauterborn, Cinematographic observation of the collapse and rebound of a laser-produced cavitation bubble near a wall, J. Fluid Mech. 479 (2003) 327–348, https://doi.org/10.1017/S0022112002003695.
[9] W. Lauterborn, T. Kurz, Physics of bubble oscillations, Rep. Prog. Phys. 73 (2010) 106501, https://doi.org/10.1088/0034-4885/73/10/106501.
[10] G.N. Sankin, P. Zhong, Interaction between shock wave and single inertial bubbles near an elastic boundary, Phys. Rev. E - Stat. Nonl. Soft Matter Phys. 74 (2006) 1–4, https://doi.org/10.1103/PhysRevE.74.046304.
[11] A. Philipp, W. Lauterborn, Cavitation erosion by single laser-produced bubbles, J. Fluid Mech. 361 (1998) 75–116, https://doi.org/10.1017/S0022112098008738.
[12] Y. Zhang, F. Chen, Y. Zhang, Y. Zhang, X. Du, Experimental investigations of interactions between a laser-induced cavitation bubble and a spherical particle, Exp. Therm. Fluid Sci. 98 (2018) 645–661, https://doi.org/10.1016/j.expthermflusci.2018.06.014.
[13] D. Obreschkow, M. Tinguely, N. Dorsaz, P. Kobel, A. De Bosset, M. Farhat, Universal scaling law for jets of collapsing bubbles, Phys. Rev. Lett. 107 (2011) 3–6, https://doi.org/10.1103/PhysRevLett. 107.204501.
[14] K.S.F. Lew, E. Klaseboer, B.C. Khoo, A collapsing bubble-induced micropump: an experimental study, Sens. Actuat. A Phys. 133 (2007) 161–172, https://doi.org/10.1016/j.sna.2006.03.023.
[15] C.F. Naudé, A.T. Ellis, On the mechanism of cavitation damage by nonhemispherical cavities collapsing in contact with a solid boundary, J. Basic Eng. 83 (1961) 648, https://doi.org/10.1115/1.3662286.
[16] Y. Tomita, A. Shima, Mechanisms of impulsive pressure generation and damage pit formation by bubble collapse, J. Fluid Mech. 169 (1986) 535–564, https://doi.org/10.1017/S0022112086000745.
[17] A.M. Zhang, P. Cui, Y. Wang, Experiments on bubble dynamics between a free surface and a rigid wall, Exp. Fluids 54 (2013), https://doi.org/10.1007/s00348-013-1602-7.
[18] Y. Tomita, Interaction of a shock wave with a single bubble, Shock Wave Sci. Technol. Ref. Libr. Springer Berlin Heidelberg, Berlin, Heidelberg, 2007, pp. 35–66, , https://doi.org/10.1007/978-3-540-35846-6_2.
[19] T. Kodama, K. Takayama, N. Nagayasu, The dynamics of two air bubbles loaded by an underwater shock wave, J. Appl. Phys. 80 (1996) 5587–5592, https://doi.org/10.1063/1.363605.
[20] T. Kodama, Y. Tomita, Cavitation bubble behavior and bubble-shock wave interaction near a gelatin surface as a study of in vivo bubble dynamics, Appl. Phys. B Lasers Opt. 70 (2000) 139–149, https://doi.org/10.1007/s003400050022.
[21] T. Kodama, K. Takayama, Dynamic behavior of bubbles during extracorporeal shock-wave lithotripsy, Ultrasound Med. Biol. 24 (1998) 723–738, https://doi.org/10.1016/S0301-5629(98)00022-2.
[22] A. Philipp, M. Delius, C. Scheffczyk, A. Vogel, W. Lauterborn, Interaction of lithotripter-generated shock waves with air bubbles, J. Acoust. Soc. Am. 93 (1993) 2496–2509, https://doi.org/10.1121/1.406853.
[23] C.D. Ohl, R. Ikink, Shock-wave-induced jetting of micron-size bubbles, Phys. Rev. Lett. 90 (2003) 4, https://doi.org/10.1103/PhysRevLett. 90.214502.
[24] S. Fujikawa, T. Akamatsu, Experimental investigations of cavitation bubble collapse by a water tube, Japan Soc. Mech. Eng. 21 (1978) 223–230.
[25] K. Vokurka, The use of a shock tube in bubble dynamics studies, Czechoslov. J. Phys. 42 (1992) 291–302, https://doi.org/10.1007/BF01598426.
[26] J.P. Dear, J.E. Field, A study of the collapse of arrays of cavities, J. Fluid Mech. 190 (1988) 409–425, https://doi.org/10.1017/S0022112088001387.
[27] A.B. Swantek, J.M. Austin, Collapse of void arrays under stress wave loading, J. Fluid Mech. 649 (2010) 399–427, https://doi.org/10.1017/S0022112009993545.
[28] J.D. Anderson, Modern Compressible Flow: With Historical Perspective, McGraw-Hill, New York, 1990.
[29] P. Cui, Q.X. Wang, S.P. Wang, A.M. Zhang, Experimental study on interaction and coalescence of synchronized multiple bubbles, Phys. Fluids 28 (2016), https://doi.

org/10.1063/1.4939007.
[30] G.S. Settles, Schlieren and Shadowgraph Techniques, Springer Berlin Heidelberg, Berlin, Heidelberg, 2001https://doi.org/10.1007/978-3-642-56640-0.
[31] L. Brekhovskikh, Waves in Layered Media, Elsevier, 2012.
[32] J.P. Dear, J.E. Field, A.J. Walton, Gas compression and jet formation in cavities collapsed by a shock wave, Nature 332 (6164) (1988) 505–508, https://doi.org/10.1038/332505a0 http://www.nature.com/articles/332505a0https://doi.org/10.1038/332505a0.
[33] N.K. Bourne, J.E. Field, Shock-induced collapse of single cavities in liquids, J. Fluid Mech. 244 (1992) 225–240, https://doi.org/10.1017/S0022112092003045.
[34] N.K. Bourne, J.E. Field, Shock-induced collapse and luminescence by cavities, R. Soc. 357 (1999) 295–311.
[35] E.A. Brujan, P.R. Williams, Cavitation phenomena in non-Newtonian liquids, Chem. Eng. Res. Des. 84 (2006) 293–299, https://doi.org/10.1205/cherd05054.
[36] A.V. Bazilevskii, D.D. Meier, A.N. Rozhkov, Dynamics of a spherical microcavity in a polymeric liquid, Fluid Dyn. 38 (2003) 351–362.
[37] P.B. Deasy, K.J. Quigley, Rheological evaluation of deacetylated gellan gum (Gelrite) for pharmaceutical use, Int. J. Pharm. 73 (1991) 117–123, https://doi.org/10.1016/0378-5173(91)90034-L.
[38] L.W. Chew, E. Klaseboer, S.W. Ohl, B.C. Khoo, Interaction of two differently sized oscillating bubbles in a free field, Phys. Rev. E - Stat. Nonl. Soft Matter Phys. 84 (2011), https://doi.org/10.1103/PhysRevE.84.066307.
[39] B. Han, K. Köhler, K. Jungnickel, R. Mettin, W. Lauterborn, A. Vogel, Dynamics of laser-induced bubble pairs, J. Fluid Mech. 771 (2015) 706–742, https://doi.org/10.1017/jfm.2015.183.